

Formation Control Algorithm for Multiple Mobile Robots Based on Fuzzy Mathematics

Bingqian Fan

Artificial Intelligence and Big Data College, Hebei University of Engineering Science, Langfang 050000, China

E-mail: lingbingyang888@163.com

Keywords: fuzzy sliding mode, mobile robots, formation, kinematics model

Received:

The formation of multiple mobile robots suffers from unsmooth formation trajectory tracking and large formation control errors. A three closed-loop sliding mode formation control method was proposed to solve these problems, which achieved stable three closed-loop control systems from both linear and angular velocity directions. Meanwhile, fuzzy theory was introduced to design a fuzzy sliding mode control model for multiple mobile robots, which made the gain switching smoother, and the problems of unsmooth and interference were solved in trajectory tracking. The results showed that the linear velocity fluctuation of the research designed model was controlled within 5 seconds, and the angular velocity fluctuation was controlled within 1 second. The overall mean value of position control indicators was 17.08, which was smaller than the comparison model. The average value of the comprehensive control index of position and speed was 2.8, which was smaller than the comparison model. The model designed in this research had higher control accuracy and more stable control effects, ensuring the efficient and high-quality execution of tasks by robots. This research provides a technical basis for the formation motion control of multiple mobile robots.

Povzetek: Raziskava izboljšuje formacijsko kontroliranje mobilnih robotov s trojno zaprto zanko in uvajanjem mehke logike za gladko preklapljanje ojačitve.

1 Introduction

With the development of modern technology, automated robots begin to occupy an important position in extreme conditions, large-scale labor, and even military operations assistance. Due to the complexity of the task content, a single-robot cannot efficiently complete tasks, so multiple mobile robot formation and collaborative work becomes a main method. Multiple mobile collaboration has obvious advantages over single-robot operations, such as the ability to complete more complex positioning tasks through collaborative operations, decompose tasks, and improve work efficiency. Meanwhile, multiple mobile collaboration can flexibly process tasks, and improve job fault tolerance [1-3]. However, in the current robot collaborative formation operations, it is easy to encounter problems such as insufficient control accuracy, low adaptive ability, and inefficient adjustment. How to efficiently and reasonably coordinate task allocation and formation marching is a challenging issue, especially when multiple robots can complete a task with only the difference of the path length and time. In a positional environment, the robot's judgment of its task execution ability is not only based on its own functional judgment, but also depends on the robot's perception of the external environment and self-positioning in the environment [4-6]. In the presence of multiple robots, sensors are needed to jointly locate robots, thereby laying the foundation for formation control and collaborative

operations. However, the external real-time environment is often in a dynamically changing environment. The formation motion of multiple mobile robots is likely to be strongly interfered with by the outside world, greatly increasing the difficulty of robot motion control [7-9]. Therefore, the automation technologies are needed to help robots achieve accurate trajectory tracking based on robot motion status, thereby completing high-precision formation of multiple mobile robots. To this end, a three closed-loop sliding mode formation control method based on fuzzy mathematics was proposed in this study, which smoothed the switching gain by designing fuzzy rules. In practical environments, this control method can significantly reduce the jitter problem of sliding mode control and improve the stability of robot formations. Therefore, this method can be applied in areas such as heavy object handling, military operation assistance, post disaster search and rescue, and automated chemical plants. The research provides theoretical guidance for the theoretical research and hardware development of multiple mobile robot formation control. This paper also lays a good foundation for the mutual cooperation between robots to achieve navigation, positioning, and obstacle avoidance.

2 Related works

In recent years, research on robot formation is continuously enriched. Liu et al. proposed a bilateral consistent robot formation control protocol for complex

agent systems. This technology extended the third-order bilateral protocol to achieve bilateral consistency in higher-order states. Meanwhile, the asymptotic stability of this system was achieved by adjusting the gain parameters of the system. At the same time, the essential relationship between each state variable and the gauge transformation in the system was analyzed. Research results showed that this technology achieve effective control in multiple robot formation [10]. Khalaji and Zahedifar proposed a nonlinear dynamic model for autonomous underwater robots and designed a formation motion algorithm for underwater robots based on the model. This algorithm was more robust than traditional algorithms, which achieved efficient utilization of resources under limited resource conditions. The research results showed that the model arranged different formations and motion paths for underwater robots, which was effective [11]. Dai et al. proposed a constrained multiple robot formation system based on uncertain dynamic models. The formation system achieved time-varying robot formation tracking from both relative distance and relative azimuth through visual technology. A recursive adaptive technique was proposed to solve the constraint problem, which converged the formation to a small area near the origin under limited time constraints. The research results showed that this model effectively achieved formation control [12]. Kamel et al. analyzed the formation control and coordination strategy for unmanned vehicles. First, the formation control for two different situations of ground unmanned vehicles, namely, normal and fault conditions, was defined and analyzed. Then the cooperative control of fault tolerance for vehicles with faults was analyzed [5]. Hu et al. conducted research on cooperative control and developed a coordination framework with unified clustering for robots. The framework was divided into two main levels, namely, the leadership and the follower. The model clustered and scheduled robots based on the spatial location and priority of robot targets. The research results showed that the model designed in the study was formed around the target point in accordance with the requirements [13].

On the other hand, the research on fuzzy sliding mode control has also increased. Qu et al. applied fuzzy sliding mode control to wireless sensor networks of the Internet of Things. Meanwhile, a new congestion control algorithm was proposed for wireless sensor networks. The algorithm combined fuzzy control with sliding mode control, so that the controller adjusted the buffer queue length adaptively. The research results showed that this

model converged quickly and had lower packet loss rate and latency [14]. Fei et al. proposed a micro-gyroscope control method based on adaptive fractional sliding mode control, which used a double-recursive network structure to calculate the disturbance generated by the system. At the same time, a fractional order term was added to the sliding mode surface to allocate additional degrees of freedom. An adaptive law that automatically updated free parameters was also designed. The research results showed that the model designed in the study had higher accuracy and stronger instantaneous response ability [15]. Li et al. analyzed the trajectory tracking control of the four-wheel legged robot, researched and designed a horizontal line control technology for the wheel legged robot. The fuzzy sliding mode control was used to control the slip angle and yaw angle of robots. Meanwhile, the simulation analysis was conducted by mobile robot control experiments. The research structure showed that the technology had high stability and trajectory tracking accuracy [16]. Teng et al. designed a control scheme for the upper limb exoskeleton of the wheelchair, which combined the proportional differential equation with sliding mode control. This control scheme solved the dynamic uncertainty in the human exoskeleton control. The sliding mode control was divided into equivalent and switching controls. PD controller was used in the equivalent part, while fuzzy logic control was used in the switching control part. The research results showed that this method was very effective [17]. Cao et al. designed a sliding mode controller to detect relevant events. The controller used additional internal control variables to achieve adaptive adjustment of event trigger conditions and relax the reachability conditions and stability conditions of the model. At the same time, the minimum power was optimized through the internal dynamic variable coefficient control of high-dimensional grid. The research results showed that this method performed better in simulation experiments [18]. From recent research, robot formation control accuracy is an important concern, and robot formation requires the high adaptability and control stability of the system. However, the current robot formation control accuracy method still cannot improve the uneven trajectory tracking, which only controls the linear speed, ignoring the control of angular speed. The fuzzy sliding mode control meets the adaptability and stability at the same time, so the research applied the fuzzy Sliding mode control to the robot formation control technology, providing a new idea for related fields. The literature summary of the related works is shown in Table 1.

Table 1: Summary of the literature

Author	Method	Contribute
Liu et al. [10]	Bilateral consistent robot formation control protocol for hybrid agent systems	Expanded the third-order bilateral protocol to achieve bilateral consistency in high-order states
Khalaji and Zahedifar [11]	Nonlinear dynamic model	Effectively utilized resources under limited resource conditions, and

Dai et al. [12]	Constrained multiple robot formation system based on uncertain dynamic model	arranged different formations and motion paths for underwater robots Implemented time-varying robot formation tracking in terms of relative distance and relative azimuth
Kamel et al. [5]	Formation control and coordination strategy of unmanned aerial vehicles	Defined and analyzed formation control of ground unmanned aerial vehicles under two different scenarios: normal and faulty
Hu et al. [13]	A coordinated framework for unified clustering of robots	Capable of clustering and scheduling robots based on their spatial location and priority
Qu et al. [14]	Congestion control algorithm for wireless sensor networks based on fuzzy sliding mode control	Combined the fuzzy control and sliding mode control, enabling the controller to adaptively adjust the buffer queue length
Fei et al. [15]	Control method of micro-gyroscope based on adaptive fractional sliding mode control	Enhanced the accuracy and instantaneous response capability of the gyroscope
Li et al. [16]	Horizontal line control technology of wheeled foot robot based on fuzzy sliding mode control	Improved control stability and trajectory tracking accuracy
Teng et al. [17]	A control scheme for upper limb exoskeleton combining proportional differential equation and sliding mode control	Solved the dynamic uncertainty problem in human exoskeleton control
Cao et al. [18]	Sliding mode controller	Adaptive adjustment of event triggering conditions using additional internal control variables

3 Multiple mobile robots formation control based on fuzzy mathematics

3.1 Multiple mobile robots formation and three closed-loop sliding mode formation control

The multiple robot formations are a prerequisite for formation. Only when each robot determines and

accurately and quickly moves to its own target point to complete the formation of the formation, can the robot complete the established tasks based on the initial formation. This paper proposes a target point allocation algorithm using auction mechanism regarding to the issues faced by current target point allocation algorithms such as complex computation, large path consumption, and low efficiency. The target point allocation algorithm flow is shown in Figure 1.

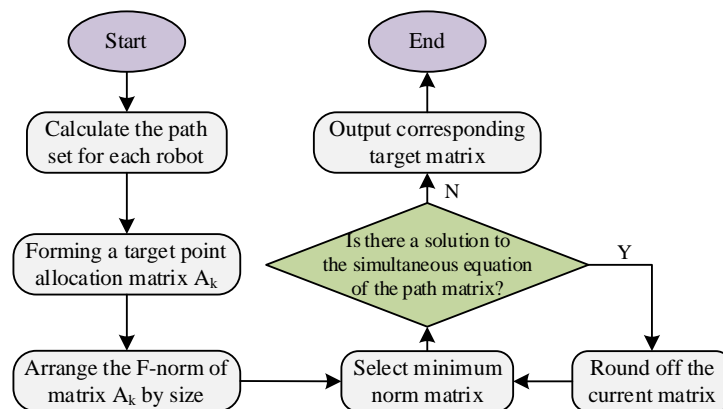


Figure 1: Target point allocation algorithm flow

The number of robots participating in the formation is set as i , and the target number of points is j , $i \leq j = 1, 2, \dots, n$, $n \in N^+$. The initial position point coordinates of the robot is recorded as (x_{i0}, y_{i0}) . The target point position coordinates is recorded as (x_{jm}, y_{jm}) . The distance l is calculated from the initial position to each target point. Equation (1) means that the connection between the points does not pass through an obstacle.

$$l_{ij} = \sqrt{(x_{jm} - x_{i0})^2 + (y_{jm} - y_{i0})^2} \quad (1)$$

When the connecting line between the initial position point and each target point passes through an obstacle, the turning path of robot is set as a semicircular arc, and the impact radius of the obstacle is r . The calculation of the path length is as shown in Equation (2).

$$l_{ij} = \sqrt{(x_{jm} - x_{i0})^2 + (y_{jm} - y_{i0})^2} - 2r + \pi r \quad (2)$$

The path length set of each robot to the target point is $L_i = \{l_{i1}, l_{i2}, \dots, l_{ij}\}$. A path element is randomly selected from each path set L_{ij} without repetition to form multiple assignment matrices C , $k = \{1, 2, \dots, n\}$. The corresponding target point positions of the selected path elements do not coincide. The F norm $\|A_k\|_F$ of each allocation matrix A_k is solved and arranged from smallest to largest. The matrix corresponding to the minimum F norm is the shortest matrix of the total path to the target point. This matrix is selected as the optimal target point assignment matrix for the current prediction, and the collision between robots in the current optimal prediction matrix is judged. According to the selected shortest path matrix, the real-time coordinate equations of the motion trajectory during the formation initialization process of each robot are listed as shown in

Equation (3).

$$\begin{cases} x_{1t} = vt|\cos \theta_1| + x_{10} \\ y_{1t} = vt|\sin \theta_1| + y_{10} \\ \vdots \\ x_{it} = vt|\cos \theta_i| + x_{i0} \\ y_{it} = vt|\sin \theta_i| + y_{i0} \end{cases} \quad (3)$$

In Equation (3), the position coordinate of robot i at moment t is (x_{it}, y_{it}) . θ_i represents the included angle between the line from the initial coordinate point of i to its corresponding target point and the positive direction of the coordinate system X axis. v represents the constant running speed of the robot. Two of the equation sets are selected in Equation (3) in the order of arrangement and combination to form a new equation set. t is then calculated. It is determined whether the two machines corresponding to the new set of equations will collide in the path based on the obtained result. If there is no time t in all new equations that can make the equations hold, then there will be no collisions between all the robots. At this time, the selected matrix is the final target point allocation matrix, and the target point allocation for robot formation initialization is completed. If there is a t that holds the equation set, collisions will occur between robots. It is necessary to discard the previously selected matrix and select the formation matrix corresponding to the next norm according to the order of data size as the new optimal prediction matrix. Then the corresponding equation set is listed to determine whether there is a collision between robots and humans until the robot target point allocation is completed.

The kinematics model is established with the laboratory wheeled robot as a reference, as shown in Figure 2.

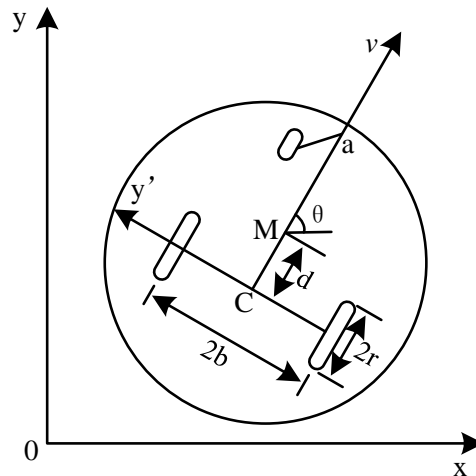


Figure 2: Kinematic model

$$\begin{bmatrix} \dot{x}_i \\ \dot{y}_i \\ \dot{\theta}_i \end{bmatrix} = \begin{bmatrix} \cos \theta_i & d \sin \theta_i \\ \sin \theta_i & -d \cos \theta_i \\ 0 & 1 \end{bmatrix} \begin{bmatrix} v_i \\ w_i \end{bmatrix} + D_i \quad (4)$$

In Figure 2, C represents the geometric center of the axis connecting the two wheels of the robot. $2b$ represents the wheels distance. r represents the wheels radius. M is the mass center of robot. θ_i is the heading angle of the robot. w_i is the wheels angular velocity. v_i is the wheels linear velocity. d is the distance between the center of mass and the geometric center. According to the kinematics model, the kinematics equation of the robot under the condition of external interference is calculated as Equation (4).

In Equation (4), D_i is the unknown disturbance, and $D_i = [D_x D_y D_\theta]^T$. Aiming at the excessive dependence on navigators of following robots, the virtual navigator method is used to optimize the formation of multiple wheeled mobile robots. It is assumed that all the i robots participating in the formation are followers, $i = 1, 2, \dots, n$. n is the total number of robots in the formation. A point is taken on the geometry that will form a fixed formation as a reference point, which is the virtual navigator of each robot, as shown in Figure 3.

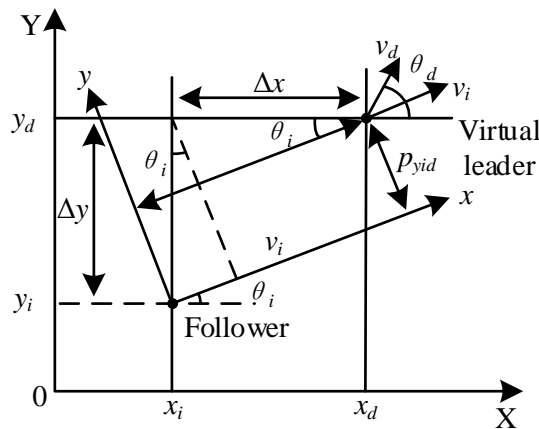


Figure 3: Virtual leader model

Assuming that the reference positions of a given virtual navigator are $q_d = [x_{id} y_{id} \theta_{id}]^T$, $u_d = [v_{id} w_{id}]^T$. The position of the following robot can be obtained from the virtual navigator model as $q_i = [x_i y_i \theta_i]^T$, $u_i = [v_i w_i]^T$. The relative position between the following robot and the virtual navigator is as shown in Equation (5).

$$P_{id} = [p_{xid} p_{yid} p_{\theta id} p_{vid} p_{wid}]^T \quad (5)$$

$\mu_{id} = [\mu_{xid} \mu_{yid} \mu_{\theta id} \mu_{vid} \mu_{wid}]^T$ is defined as the

reference ideal value of the relative position, and the relative error variance is shown in Equation (6).

$$e_{id} = P_{id} - \mu_{id} \quad (6)$$

The design goal is a control rate that $P_{id} - \mu_{id} \rightarrow 0$, enabling the tracking robot to quickly and accurately track the navigator. The three closed-loop control is realized for the wheeled robot's position subsystem and linear and angular speed subsystem by designing the linear speed control rate, position control rate, and attitude control rate. Meanwhile, this control is realized by constructing the corresponding position subsystem controller, linear speed subsystem controller, and angular speed subsystem controller. The control principle is shown in Figure 4.

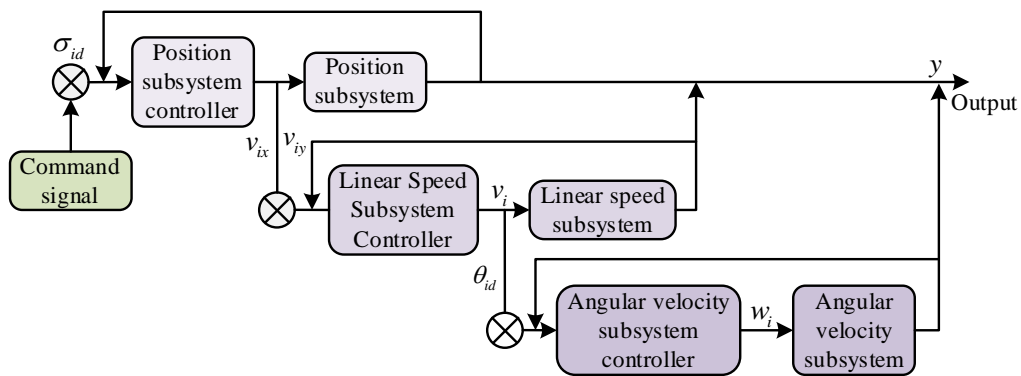


Figure 4: Three closed-loop control principle

Linear and angular velocities are controlled variables. The position (x, y, θ) and velocities v and w of the robot are output. According to the two components of the linear velocity and the relative position, the linear velocity is given, thus the heading angle and the actual linear velocity are obtained. At the same time, the actual position of the robot is deduced according to the kinematics equation. In this system, the angle and angular speed control is set as the inner loop, the linear speed control is set as the middle loop, and the position coordinate adjustment is set as the outer loop. The convergence speed is set to be greater in the inner loop than in the middle loop and greater in the middle loop than in the outer loop to ensure the stability of the three closed-loop control.

3.2 Fuzzy sliding mode formation control optimization for multiple mobile robots

The classical sliding mode controller is robust to model uncertainty and external disturbances, and the switching function can ensure the asymptotic stability of the system. But this function also causes the system jitter, resulting in an unsmooth tracking curve. One way to solve the system

jitter is to insert a saturation function in the boundary layer near the sliding surface. However, this method will affect the stability of the closed-loop system. The combination of fuzzy system and sliding mode controller can solve this problem. Fuzzy rules can make the fuzzy system approach any continuous function. The fuzzy system needs a large number of fuzzy rules to approach the time-varying nonlinear system, which leads to an increase in the amount of computation and slows down the response speed of the system. The fuzzy adaptive law is added to the sliding mode controller. The parameters of the fuzzy rule are adjusted online to ensure proper calculation, which can slow down the system jitter and accelerate its response. The laboratory wheeled robot used in the study mainly consists of two rear wheels and a front wheel, with the rear wheel responsible for driving and the front wheel responsible for balancing the system and controlling steering. The input control signals of the control system act on the left and right wheels, respectively. Assuming that the range of motion of the robot is within an ideal plane, its dynamic model is shown in Figure 5.

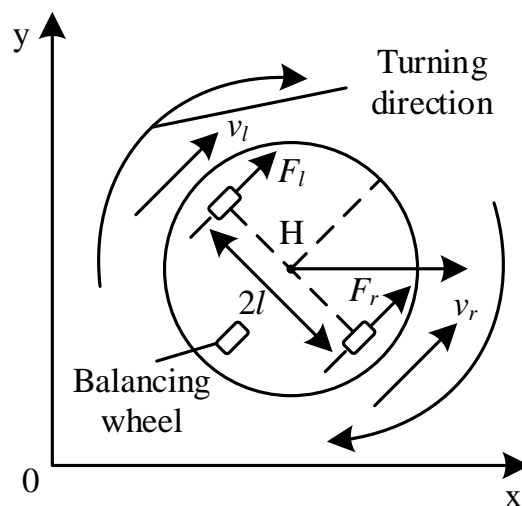


Figure 5: Dynamic model of mobile robot

A dynamic analysis on Figure 5 is performed to obtain Equation (7).

$$\begin{cases} j\beta = M_r - M_l \\ Ma = F_r - F_l \end{cases} \quad (7)$$

In Equation (7), j is the rotational inertia of the robot rotating around the central axis. M represents the mass of the robot. β and a represent angular acceleration and linear acceleration. F_l and F_r represent the forces exerted on the left and right wheels. M_l and M_r represent the torque. A balance analysis is performed on the torque of the two wheels of the robot to obtain a dynamic characteristic formula as shown in Equation (8).

$$\begin{cases} ku_l - rF_l + d_l = J\hat{\theta}_l + \omega\dot{\theta}_l \\ ku_r - rF_r + d_r = J\hat{\theta}_r + \omega\dot{\theta}_r \end{cases} \quad (8)$$

In Equation (8), θ_l and θ_r are the rotation angles of the left and right wheels. J represents the rotational inertia of the robot wheel. ω represents the viscous damping coefficient. k and r are the amplification factor and wheel radius. u_l and u_r represent the input torque of the left and right wheels. d_l and d_r represent the disturbance torque of the left and right wheels of the robot, respectively. The simplified kinematics equation of the mobile robot system can be obtained by combining Equations (7) and (8) as shown in Equation (9).

$$\begin{bmatrix} \dot{x} \\ \dot{y} \\ \dot{\theta} \end{bmatrix} = \begin{bmatrix} \cos\theta & 0 \\ \sin\theta & 0 \\ 0 & 1 \end{bmatrix} \begin{bmatrix} v_i \\ w_i \end{bmatrix} \quad (9)$$

Each robot maintains a certain distance and angle with the virtual navigator to achieve formation by using virtual navigation robots as reference points. According to the relative motion model of the virtual navigation robot and the following robot, it is assumed that the positions of the virtual navigation robot are $q_d = [x_d, y_d, \theta_d]^T$ and $u_d = [v_d, w_d]^T$. The positions of the following robot are $q_i = [x_i, y_i, \theta_i]^T$ and $u_i = [v_i, w_i]^T$, and the relative position between the two is $P = [p_{xid}, p_{yid}, p_{\theta id}]^T$. From this, the relative position formula between the two is shown in Equation (10).

$$P_{id} = \begin{bmatrix} p_{xid} \\ p_{yid} \\ p_{\theta id} \end{bmatrix} = \begin{bmatrix} \Delta x \cos\theta_i + \Delta y \sin\theta \\ \Delta y \cos\theta_i + \Delta x \sin\theta \\ \theta_d - \theta \end{bmatrix} \quad (10)$$

The input and output quantities and control objectives are determined to more intuitively characterize the control system, and the control system dynamics state equation is obtained as shown in Equation (11).

$$\hat{p} = f(\dot{p}, p) + B(p)u + C(p)d(t) + D \quad (11)$$

In Equation (11), P represents the output of the relative position. u represents control input. $d(t)$ represents unknown disturbance. If $\sigma_r = [\sigma_{xid}, \sigma_{yid}, \sigma_{\theta id}]^T$ is defined as the ideal value of the relative position, the tracking error is $e = p_{id} - \sigma_{id}$, and the second derivative is calculated to obtain Equation (12).

$$\bar{e} = \hat{p}_{id} - \hat{\sigma}_{id} \quad (12)$$

The formation task of the robot is completed by designing a control rate to maintain a certain distance and angle between the following robot and the virtual navigation robot. It is ensured that the robot does not shake during the movement process, and the stable operation of the formation is maintained with a certain control accuracy. The switching function is set for the fuzzy sliding mode controller design in Equation (13).

$$\begin{aligned} s &= Ce + \dot{e}, C \\ &= dg[c_1, c_2, \dots, c_n] \end{aligned} \quad (13)$$

Equation (13) is derived to obtain Equation (14).

$$\dot{s} = C\dot{e} + \ddot{e} = C\dot{e} + \hat{p}_{id} - \hat{\sigma}_{id} \quad (14)$$

According to Equations (13) and (14), the sliding mode control rate can be obtained as shown in Equation (15).

$$\eta = \tilde{\sigma}_{id} - C\dot{e} - \hat{p}_{id} + B(p)u + \varepsilon \operatorname{sgn}(s) + s \quad (15)$$

In Equation (15), the sliding mode control rate is $\eta = B(p)u$ and ε represent switching gain. For the control system jitter caused by switching gain, it is necessary to set the switching gain to a variable amount and be able to offset the impact of various uncertain factors such as external interference. The value $q(t)$ of switching gain ε that varies with time t is achieved through fuzzy rules, and the control rate is obtained by replacing ε with $q(t)$ as shown in Equation (16).

$$\eta = \tilde{\sigma}_{id} - C\dot{e} - f(\dot{p}, p) - C(p)d(t) - D + q(t)\operatorname{sgn}(s) + s \quad (16)$$

After proving the stability, the structure of the fuzzy sliding mode control system can be obtained as shown in Figure 6.

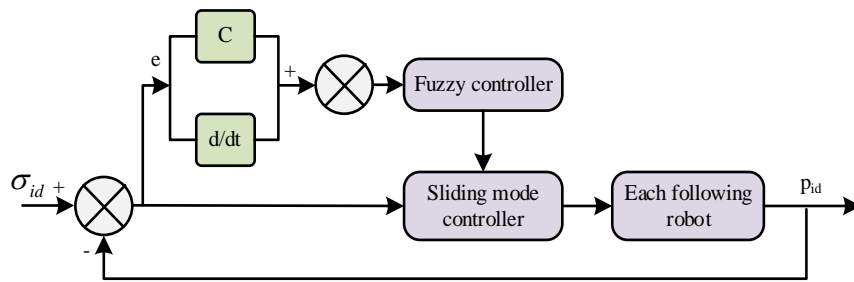


Figure 6: Fuzzy sliding mode control system structure

4 Multiple mobile robots formation control effect

Experimental analysis was conducted on the performance of the fuzzy sliding mode formation control algorithm to verify the effectiveness of this control algorithm. Assuming that the number of robots participating in the formation was 3, the system control parameters M was taken as 20 kg, j as 0.162 kg·m², and J as 0.1 kg·m². In addition, l was taken as 0.27 m, r as 0.1 m, $k=1$, and $c=0.01$. It was assumed that the linear velocity of the robot was 1 m/s, the angular velocity was 0.6 rad/s, and the input disturbances were

$d_1 = \sin(t) + \cos(t)$ N/m, $d_2 = \sin(t) - \cos(t)$ N/m, and $C = [10, 10, 10]^T$. The radius of influence of obstacles was 0.04 m, and the length of the allocation path corresponding to each target point allocation matrix was 28.2035 m. The longest path between the robot and the target point was 10.6301 m, and the initialization time was 5.3150 s. In addition, due to the order of magnitude of the control error was small, t-test was used to verify whether the control error of different algorithms is significantly different. The simulation control effect of the research model is shown in Figure 7.

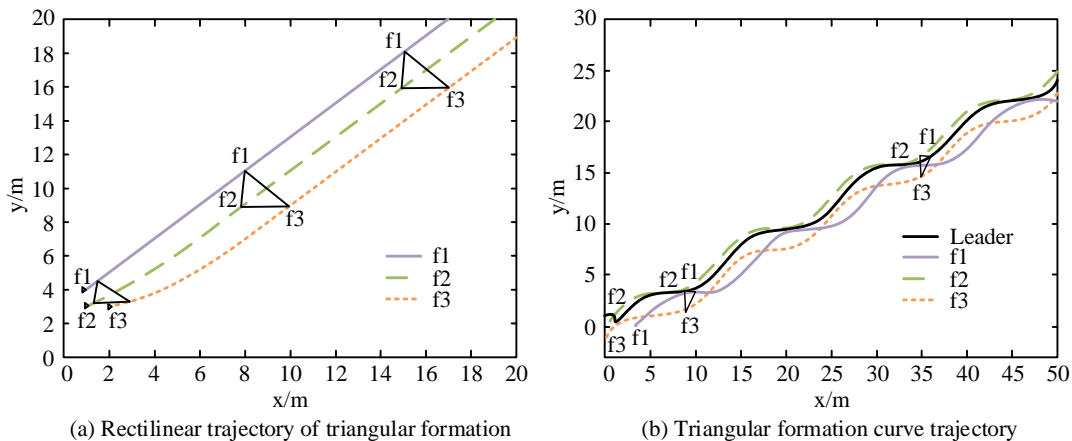


Figure 7: Movement trajectory of triangular formation

Figure 7(a) shows the formation movement in a linear trajectory, while Figure 7(b) shows the same in a curved trajectory. The f1, f2, and f3 in the figure represent three different detection points. The formation motion of robots was effectively detected by detecting the three endpoints. From the formation and movement of multiple mobile robots under linear trajectory, the research model-controlled robots to form a smooth movement trajectory. At the same time, no robots fell behind during the movement process, and the formation was maintained in good condition. From the formation and movement of multiple mobile robots under curved trajectories, the model designed in the study-controlled

robots to form a smooth curvilinear motion trajectory. Even when the motion trajectory intersected with each other, the mobile robots still completed the formation and maintained the formation intact during movement without the phenomenon of robots falling behind. In this study, Fast Adaptive Gain Nonsingular Terminal Sliding Mode Control (FAGNTSMC) was selected as the main comparison algorithm, which was recorded as F algorithm. These algorithms were compared from two aspects of speed tracking error and position tracking error. The speed tracking error curve of the model designed in the study is shown in Figure 8.

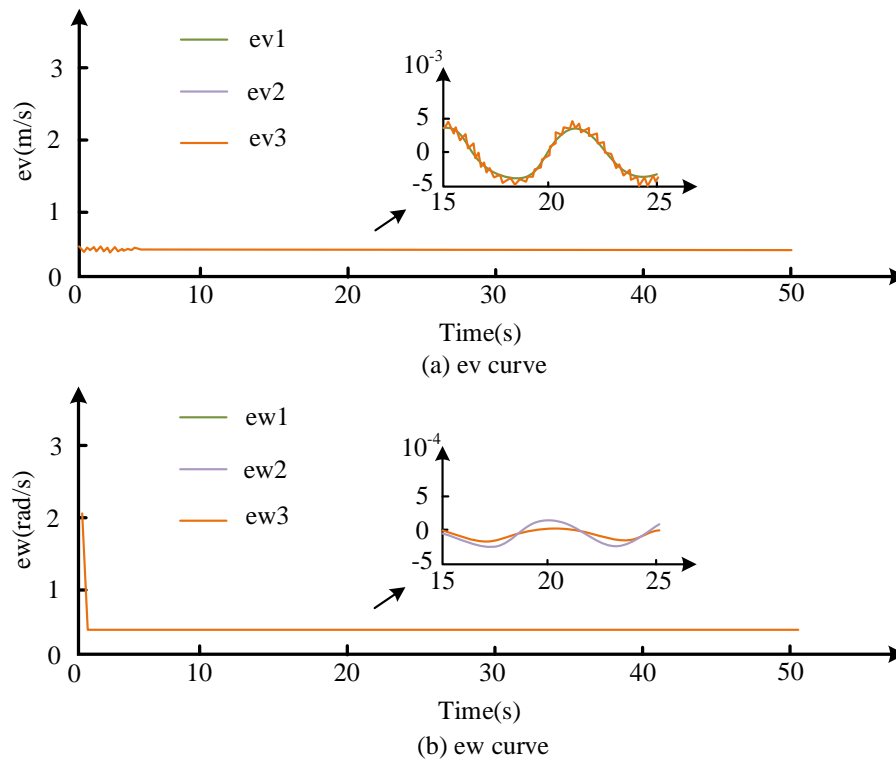


Figure 8: The speed tracking error curve study of the design model

Figure 8(a) shows the average linear velocity tracking error, and Figure 8(b) shows the average angular velocity tracking error. From the average error curve of linear velocity tracking, the linear velocity tracking curve of the formation of multiple mobile robots quickly entered a smooth state after a brief fluctuation under the control of the research model over time. The fluctuation range was between 0 s and 5 s, and after 5 s, it was a smooth range. At the same time, within the fluctuation range of 0 s to 5 s, the longitudinal fluctuation amplitude of the speed tracking curve was also very small, showing a small and dense fluctuation state. The model designed in the study overcame the jitter problem, achieved smooth

operation in a very short time, and maintained high accuracy and stability in operation. From the average error curve, the angular velocity tracking curve of a multiple mobile robot formation quickly entered a smooth state after a sudden descent over time under the control of the designed model with a sudden decent interval of 0 s to 1 s, and a smooth interval after 1 s. Among them, 1 s was the time to start adjusting the angular velocity. The designed model achieved high accuracy and stable operation in angular velocity control, which quickly reached a stable operation state. The speed tracking error curve of the F algorithm is shown in Figure 9.

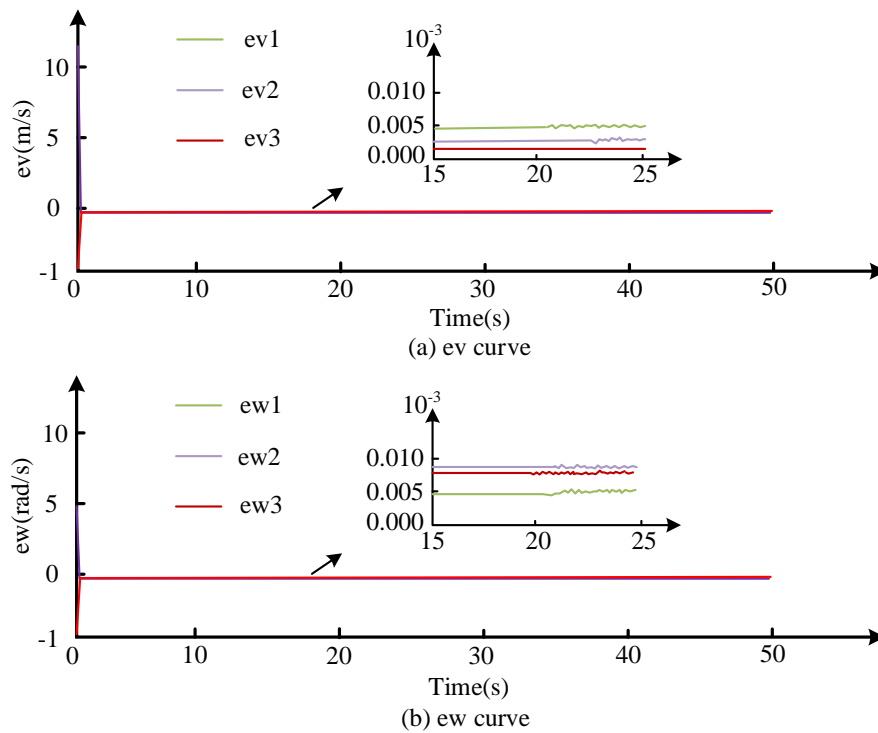


Figure 9: Speed tracking error curve of F-algorithm

Figure 9(a) shows the average linear velocity tracking error, and Figure 9(b) shows the average angular velocity tracking error. There was a magnitude difference in the control effect between the F algorithm and the research model. The research model controlled the offline speed fluctuation between 0 m/s and 1 m/s, and the angular speed fluctuation between 0 rad/s and 2 rad/s.

The F algorithm controlled the offline speed fluctuation between 0 m/s and 10 m/s, and the angular speed fluctuation between 0 rad/s and 10 rad/s. The research model had significant performance advantages in the smooth operation control of multiple mobile robot formation. The position tracking errors are shown in Table 2.

Table 2: Position tracking error

Target	Unit	Detection Point	the Algorithm of This Research	Comparison Algorithm (F algorithm)
Avex	10^{-3} m	f1	4.5*	46.0*
		f2	4.4*	37.0*
		f3	4.8*	47.0*
		f	4.6*	43.3*
Avey	10^{-4} m	f1	3.4	3.7
		f2	3.1	2.5
		f3	1.8	3.4
		f	2.8	3.2
Avetheta	10^{-4} rad	f1	1.4*	302.0*
		f2	2.1*	243.0*
		f3	1.5*	322.0*
		f	1.7*	289.0*
Avec	10^{-4} m/rad	f	17.08*	98.58*

Note: * indicates that $P < 0.05$.

In Table 2, *Ave_x* is the absolute average position deviation of *x*, *Ave_y* is the absolute average position deviation of *y*, *Ave_θ* is the absolute average position deviation of the heading angle, and *Ave_c* represents the cheap average value. On *Ave_x*, the indicator values of the research model at detection points *f1*, *f2*, and *f3* and the average detection value *f* were 4.5, 4.4, 4.8, and 4.6. The index values of the F algorithm were 46.0, 37.0, 47.0, and 43.3. There was an order of magnitude difference in the offset value. On *Ave_y*, the indicator values of the research design model at the detection points *f1*, *f2*, and *f3* and the average detection value *f* were 3.4, 3.1, 1.8, and 2.8. The index values for the F algorithm were 3.7,

2.5, 3.4, and 3.2. Although the gap was not significant, the research model had more advantages. On *Ave_θ*, the index values of the research model at the detection points *f1*, *f2*, and *f3* and the average detection value *f* were 1.4, 2.1, 1.5, and 1.7. The index values of the F algorithm were 302.0, 243.0, 322.0, and 289.0. There was an order of magnitude difference in the offset value. On *Ave_c*, the index value of the research model was 17.08, and the index value of the F algorithm was 98.58. Overall, the research model had better performance in position shift control. From a comprehensive perspective, the speed error comparison of the two methods is shown in Figure 10.

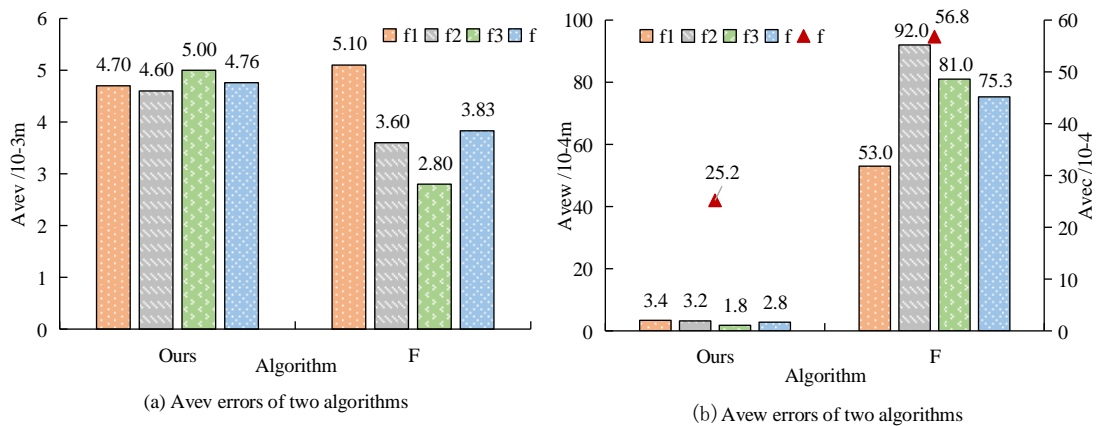


Figure 10: Velocity error of two algorithms

In Figure 10, on *Ave_v*, the index values of the research design model at *f1*, *f2*, *f3*, and *f* were 4.7, 4.6, 5.0, and 4.76. The F1 algorithms were 5.1, 3.6, 2.8, and 3.83. On *Ave_v*, the index values of the research model at *f1*, *f2*, *f3*, and *f* were 3.4, 3.2, 1.8, and 2.8. The index values of the F1 algorithm were 53, 92, 81, and 75.4. On *Ave_c*, the indicator value for the research model was 25.2. The F1 algorithm was 56.8. Overall, the model designed

in the study was slightly inferior in online speed control, mainly appearing at the *f2* point. The angular speed control effect had an order of magnitude advantage, and the overall control effect was significantly superior to the F algorithm. The control effect of the research mode was better. The comprehensive control effect of speed and position is shown in Figure 11.

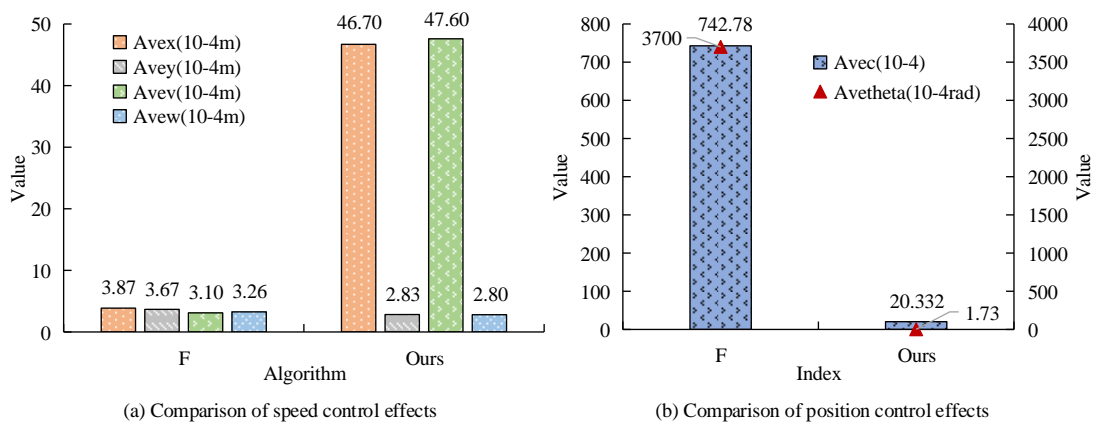


Figure 11: Comprehensive control effect of speed and position

In Figure 11, the number of *Ave_y* indicators in the research model was 2.83, the number of *Ave_θ* indicators was 1.73, and the number of *Ave_v* indicators

was 2.8, which were significantly higher than those of the F algorithm. At the same time, the number of *Ave_c* indicators was 2.8, and the F algorithm was 3.26. Based

on the comprehensive evaluation, the performance of the research model was better, which made multiple robot formation control more accurate and stable. The

performance of the proposed algorithm in the real environment is shown in Table 3.

Table 3: Control results in the actual environment

Target	Unit	Detection point	The algorithm of this research	Comparison algorithm (F algorithm)	Control accuracy	
					The algorithm of this research	Comparison algorithm (F algorithm)
Avex	10^{-3} m	f1	4.7*	47.2*	6.8	5.2
		f2	4.1*	36.0*	0.5	1.3
		f3	4.3*	48.1*	0.1	0.1
		f	4.4*	42.9*	0.2	0.8
Avey	10^{-4} m	f1	2.9	3.8	9.5*	14.4*
		f2	2.8	2.2	8.9*	13.3*
		f3	1.5	3.3	7.4	11.6
		f	2.6	2.9	8.8	10.7
Avetheta	10^{-4} rad	f1	1.3*	302.6*	10.3*	15.6*
		f2	1.9*	242.3*	9.7*	13.8*
		f3	1.5*	321.2*	11.2	13.1
		f	1.5*	289.5*	10.1*	14.2*
Avec	10^{-4} m/rad	f	16.52*	99.01*	19.5*	24.3*

Note: * indicates that $P < 0.05$.

According to Table 3, on Avex, the indicator values and the average detection value f of the research model at detection points f1, f2, and f3 were 4.7, 4.1, 4.3, and 4.4, respectively. The indicator values of the F algorithm were 47.2, 36.0, 48.1, and 42.9, respectively. There was an order of magnitude difference in the offset value. On Avey, the indicator values and the average detection value f of the research model at detection points f1, f2, and f3 were 2.9, 2.9, 1.5, and 2.6, respectively. The indicator values of the F algorithm were 3.8, 2.2, 3.3, and 2.9, respectively. Although the gap was not significant, the research model had more advantages. On Avetheta, there was an order of magnitude difference in the offset values between the research model and the F algorithm. On Avec, the indicator value for the research model was 16.52, while the indicator value for the F algorithm was 99.01. In terms of the control accuracy, the research algorithm improved by more than 10% compared to the comparative algorithm. Overall, the research model had better performance in position offset control.

5 Discussion

With the development of robotics technology, the formation control of multiple mobile robots has received much attention in recent years. At the same time, scholars have conducted much research on the poor accuracy of traditional control methods. This article also studied the problem and proposed a three closed-loop sliding mode

formation control method. The proposed method had better control stability and accuracy compared to the control methods in references [10] and [11]. This is because fuzzy theory are introduced and a fuzzy sliding mode control model is designed for multiple mobile robots, which makes the gain switching smoother and solves the unevenness and interference in track tracking. The proposed control method had better control performance compared to the control methods in references [12] and [13]. This is because the three closed-loop sliding mode formation control method can achieve stable three closed-loop control systems from both linear and angular velocities. As a result, the three closed-loop sliding mode control method has better control effect, control accuracy, and control stability.

6 Conclusion

A three closed-loop sliding mode formation control strategy was studied and designed to address the unsmooth formation trajectory tracking and large formation control errors in multiple mobile robot formations, achieving stable three closed-loop speed control. Thus, a fuzzy sliding mode control model was designed for unsmooth position control. The results showed that this model controlled the formation of multiple mobile robots to form a smooth motion trajectory. The linear speed control of the model entered a stable state after 5 seconds, and the angular speed control

entered a stable state after 1 second. The model achieved rapid and highly stable speed control. In terms of location control, the average value of the model on the Avex index was 4.6, the average value on the Avey index was 2.8, the average value on the Avetheta index was 1.7, and the average value on the overall index was 17.08. The values of all error indicators were lower than the comparison model, which showed that the research model had more advantages in position control. By integrating speed control and position control effects, the Avey index number value of the research design model was 2.83, Avetheta index number value was 1.73, Avey index number value was 2.8, and the overall index average value was 2.8, both lower than the comparison model. The model designed in the research achieved more stable, accurate, and smooth control over the speed position integrated formation control, making the formation movement of multiple robots more controllable and the task execution efficiency higher. However, the study does not consider the speed response problem for the design of the fuzzy controller. Meanwhile, the final controller is designed by the combination of fuzzy and sliding mode under the constraint of the preset function. Therefore, the fuzzy logic reasoning process may cause a delay in the response time.

References

- [1] Guan Jiansheng, Zhou Wende, Kang Shaobo, Sun Yuan, and Liu Zibo. Robot formation control based on Internet of things technology platform. *IEEE Access*, 8:96767-96776, 2020. <https://doi.org/10.1109/ACCESS.2020.2992701>
- [2] Koung Daravuth, Kermorgant Olivier, Fantoni Isabelle, and Belouaer Lamia. Cooperative multi-robot object transportation system based on hierarchical quadratic programming. *IEEE Robotics and automation letters*, 6(4):6466-6472, 2021. <https://doi.org/10.1109/LRA.2021.3092305>
- [3] Lu Peifen, Wang He, Zhang Fan, Yu Wenwu, and Chen Guanrong. Formation control of nonholonomic mobile robots using distributed estimators. *IEEE Transactions on circuits and systems II-express briefs*, 67(12):3162-3166, 2020. <https://doi.org/10.1109/TCSII.2020.2973773>
- [4] Yin He, Guo Shuxiang, and Liu Meng. A virtual linkage-based dual event-triggered formation control strategy for multiple amphibious spherical robots in constrained space with limited communication. *IEEE Sensors journal*, 22(13):13395-13406, 2022. <https://doi.org/10.1109/JSEN.2022.3175715>
- [5] Kamel Mohamed A, Yu Xiang, and Zhang Youmin. Formation control and coordination of multiple unmanned ground vehicles in normal and faulty situations: A review. *Annual reviews in control*, 49:128-144, 2020. <https://doi.org/10.1016/j.arcontrol.2020.02.001>
- [6] Dong Xiaoguang and Sitti Metin. Controlling two-dimensional collective formation and cooperative behavior of magnetic microrobot swarms. *The international journal of robotics research*, 39(5):617-638, 2020. <https://doi.org/10.1177/0278364920903107>
- [7] Fu Weiming, Qin Jiahu, Zheng Weixing, Chen Yuhang, and Kang Yu. Resilient cooperative source seeking of double-integrator multi-robot systems under deception attacks. *IEEE Transactions on industrial electronics*, 68(5):4218-4227, 2020. <https://doi.org/10.1109/TIE.2020.2987270>
- [8] Hu Junyan, Bhowmick Parijat, and Lanzon Alexander. Group coordinated control of networked mobile robots with applications to object transportation. *IEEE Transactions on vehicular technology*, 70(8):8269-8274, 2021. <https://doi.org/10.1109/TVT.2021.3093157>
- [9] Asai Ryo and Sakurama Kazunori. Cooperative reference frame estimation for multi-agent systems via formation control. *Advanced robotics*, 37(3):198-209, 2023. <https://doi.org/10.1080/01691864.2022.2119887>
- [10] Liu Dejian, Zong Chengguo, Wang Detang, Zhao Wenbin, Wang Yuehua, and Lu Wei. Multi-robot formation control based on high-order bilateral consensus. *Measurement and control*, 53(5-6):983-993, 2020. <https://doi.org/10.1177/0020294020905075>
- [11] Khalaji Ali Keymasi and Zahedifar Rasoul. Lyapunov-based formation control of underwater robots. *Robotica*, 38(6):1105-1122, 2020. <https://doi.org/10.1017/S0263574719001279>
- [12] Dai Shi-Lu, Lu Ke, and Fu Jun. Adaptive finite-time tracking control of nonholonomic multirobot formation systems with limited field-of-view sensors. *IEEE Transactions on cybernetics*, 52(10):10695-10708, 2021. <https://doi.org/10.1109/TCYB.2021.3063481>
- [13] Hu Junyan, Bhowmick Parijat, Jang Inmo, Arvin Farshad, and Lanzon Alexander. A decentralized cluster formation containment framework for multirobot systems. *IEEE Transactions on robotics*, 37(6):1936-1955, 2021. <https://doi.org/10.1109/TRO.2021.3071615>
- [14] Qu Shaocheng, Zhao Liang, and Xiong Zhili. Cross-layer congestion control of wireless sensor networks based on fuzzy sliding mode control. *Neural computing and applications*, 32(17):13505-13520, 2020. <https://doi.org/10.1007/s00521-020-04758-1>
- [15] Fei Juntao, Wang Zhe, Liang Xiao, Feng Zhilin, and Xue Yuncan. Fractional sliding-mode control for microgyroscope based on multilayer recurrent fuzzy neural network. *IEEE Transactions on fuzzy systems*, 30(6):1712-1721, 2021. <https://doi.org/10.1109/TFUZZ.2021.3064704>
- [16] Li Jiehao, Wang Junzheng, Peng Hui, Hu Yingbai, and Su Hang. Fuzzy-torque approximation-enhanced

- sliding mode control for lateral stability of mobile robot. *IEEE Transactions on systems, man, and cybernetics-systems*, 52(4):2491-2500, 2021. <https://doi.org/10.1109/TSMC.2021.3050616>
- [17] Teng Long, Gull Muhammad Ahsan, and Bai Shaoping. PD-based fuzzy sliding mode control of a wheelchair exoskeleton robot. *IEEE-ASME Transactions on mechatronics*, 25(5):2546-2555, 2020. <https://doi.org/10.1109/TMECH.2020.2983520>
- [18] Cao Zhiru, Niu Yugang, Lam Hak-Keung, Zhao Jiancong. Sliding mode control of Markovian jump fuzzy systems: A dynamic event-triggered method. *IEEE Transactions on fuzzy systems*, 29(10):2902-2915, 2020. <https://doi.org/10.1109/TFUZZ.2020.3009729>